Springer

KSME

Journal of Mechanical Science and Technology 32 (4) (2018) 1593~1600
www.springerlink.com/content/1738-494x(Print)/1976-3824(Online)
DOI 10.1007/s12206-018-0314-6

Wetting characteristics of a water droplet on solid surfaces with various pillar surface fractions under different conditions †

Min Jung Yoo[1], Matthew Stanley Ambrosia[2], Tae Woo Kwon[1], Joonkyung Jang[3] and Man Yeong Ha[1,*]

[1]*School of Mechanical Engineering, Pusan National University, Busandaehak-ro 63beon-gil, Geumjeong-gu, Busan 46241, Korea*
[2]*Department of Environmental Administration, Catholic University of Pusan, 57 Oryundae-ro, Geumjeong-gu, Busan 46252, Korea*
[3]*Department of Nanoenergy Engineering, Pusan National University, Busandaehak-ro 63beon-gil, Geumjeong-gu, Busan 46241, Korea*

(Manuscript Received May 18, 2017; Revised December 17, 2017; Accepted January 23, 2018)

Abstract

A numerical study was carried out using a molecular dynamics program to examine the wetting characteristics of nano-sized water droplets on surfaces with various pillar surface fractions under different conditions. Square-shaped pillars had surface fractions that increased from 11.1 % to 69.4 %. The pillars had 4 different heights and 3 different surface energies. When the pillar surface fraction changed, the contact angle of a water droplet also changed due to the attraction between the droplet and the pillar surface or the inner attraction of the water molecules. The pillar height also has different effects on the water droplet depending on the magnitude of surface energy.

Keywords: Contact angle; Molecular dynamics; Nano-sized pillar; Pillar surface fraction; Wetting characteristics

1. Introduction

Nano- or microscale structures can be observed on the surface of a variety of plants and animals, such as lotus leaves, water strider legs, and amphibian feet. Various enhancements of solid surfaces with nano- or microscale structures are being developed. A super-hydrophobic effect can appear on a surface with various structures. This surface can also be made using a biomimetic scheme [1-3]. There are many studies on applying these hydrophobic surfaces. Antifouling and self-cleaning surfaces can be created by using a biomimetic scheme [4]. These enhancements are used in a wide range of fields. A riblet surface that is similar to shark skin is helpful for reducing drag, which was used to develop a full-length body suit to reduce resistance in water. This concept could also be applied to aircraft or ocean vessels [5].

Contact angle measurement is the most general method for evaluating wetting. Water droplets on rough surfaces typically exhibit either a Wenzel state or a Cassie-Baxter state [6, 7]. The Wenzel model asserts that the water droplet intrudes spaces between the pillars on solid surfaces. However, there are other cases where the water droplet does not permeate into the between the pillar structures and air is trapped in the gaps instead. In these circumstances, the water rests on top of the pillar structures. This is explained by the Cassie-Baxter model.

Computational and experimental investigations have been reported on wetting phenomena, and the results have been applied to diverse fields. Many studies have focused on super-hydrophobic surfaces that are similar to lotus leaves or water strider legs [8-18]. Guo et al. [16] demonstrated wettability on super-hydrophobic surfaces. They created super-hydrophobic surfaces by applying a treatment to aluminum alloy, which had long-term stability in a wide pH range. Gao et al. [17] made an artificial hydrophobic "leg" from quartz fiber based on the non-wetting legs of water striders with similar size and shape. Using Cassie's law, they found that the air fraction between the water surface and the leg forms a cushioning effect that keeps the leg from being wetted. Wu et al. [18] designed and fabricated artificial water strider legs using a high-performance polymer with high mechanical strength and thermal stability. The legs were refined with nano-groove structures that have high water-repelling performance and thermal stability.

Koishi et al. [19] studied coexisting Wenzel and Cassie-Baxter states and transitions between them on hydrophobic pillar surfaces. They performed simulations of water droplets on pillared surfaces demonstrated both the Cassie-Baxter and Wenzel states. The state depended on the water droplet's initial location when the pillar height was very high. They also examined the free energy barrier separating the Wenzel and Cassie-Baxter states. Murakami et al. [20] investigated the

*Corresponding author. Tel.: +82 51 510 2440, Fax.: +82 51 515 3101
E-mail address: myha@pusan.ac.kr
† Recommended by Associate Editor Seongwon Kang

wetting transition of water droplets from the metastable Cassie-Baxter state to the Wenzel state on rough polymer surfaces. They investigated the wetting behaviors of solid surfaces with various pillar surface fractions using various liquids.

Many studies on wetting characteristics have used computational methods. Ambrosia et al. [21] focused on the effects of the pillar surface fractions on the wetting of a surface with nano-scale structures. Jeong et al. [22] studied the static and dynamic characteristics of a water droplet on various surfaces. They considered the effect of the pillar height, pillar gap, and an applied force.

Previous studies have been concerned with the wetting characteristics of water droplets on surfaces according to the changes of the surface texture and structures. However, there are few studies on pillar surface fractions. Pillar surface fractions were not considered or they were fixed at 25 %.

In this study, we investigated the wetting characteristics of water droplets on surfaces with various pillar surface fractions to understand the effect of surface fractions on wetting of surfaces. We control not only pillar surface fractions but also pillar heights and surface energies. And the results are compared with the shapes and contact angles.

2. Numerical method

Molecular dynamics is a computer simulation method for studying the nanoscopic movement of each atom and molecule in gas, liquid, and solid states. The open source program, nanoscale molecular dynamics (NAMD) is computer software used for molecular dynamics simulations and was developed by the University of Illinois at Urbana-Champaign [23]. It uses the CHARMM force field to calculate the interactions of molecules. This program is used for analyzing situations such as a water droplet on a solid surface. It can also be linked to visualization in molecular visualization program, visual molecular dynamics (VMD). NAMD uses a common potential energy function form:

$$U_{total} = U_{bond} + U_{angle} + U_{dihedral} + U_{LJ} + U_{Coulomb} . \quad (1)$$

The interaction between the water droplet and the solid surface is most important in this study. U_{LJ} represents the Lennard-Jones potential:

$$U_{LJ} = \sum_{i}\sum_{j>i} 4\varepsilon_{ij}\left[\left(\frac{\sigma_{ij}}{r_{ij}}\right)^{12} - \left(\frac{\sigma_{ij}}{r_{ij}}\right)^{6}\right]. \quad (2)$$

The term ε_{ij} of Eq. (2) is the characteristic energy, σ_{ij} is the characteristic length, and r_{ij} represents the distance between atoms. The Lorentz-Bertholet mixing rule determines the ε_{ij} and σ_{ij} values for different i and j:

$$\varepsilon_{ij} = \sqrt{\varepsilon_i \times \varepsilon_j} \quad (3)$$

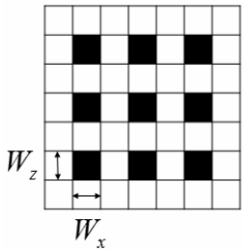

Fig. 1. Schematic view (top view) of pillar patterned surface and W_x is x-direction pillar edge and W_z is z-direction pillar edge.

$$\sigma_{ij} = (\sigma_i + \sigma_j)/2 . \quad (4)$$

The surface energy is a physical property of solid materials. It is similar to the surface tension of a liquid. It quantifies the disruption of intermolecular bonds that occur when a surface is created. The contact angle is decided by the solid surface energy and liquid surface tension. In this paper, it was controlled by using the characteristic energy of the surface and was calculated from the contact angle according to Eqs. (5) and (6) [24].

$$1 + \cos\theta = 2\sqrt{\gamma_s^d}\left(\frac{\sqrt{\gamma_w^d}}{\gamma_w}\right) + 2\sqrt{\gamma_s^h}\left(\frac{\sqrt{\gamma_w^h}}{\gamma_w}\right) \quad (5)$$

$$\gamma = \gamma^d + \gamma^h . \quad (6)$$

The term θ is the contact angle and γ is the surface tension. The subscripts *s* and *w* refer to solid and water. And, the superscripts *d* and *h* refer to the dispersion force and hydrogen bonding components.

The system uses the NVT ensemble, which is the canonical ensemble in which there is a fixed number of atoms, volume, and temperature.

Variables related to water molecules were adapted from the TIP3 model. The charge of the TIP3 oxygen atom is -0.834e, and that of the TIP3 hydrogen atom is +0.417e. The bond length between oxygen and hydrogen is 0.9572 Å, and the angle between the two hydrogen atoms is 104.52°. 3921 water molecules are used in this study.

The surface is made of a face-centered cubic (FCC) structure with a distance of 2.12 Å to the nearest neighbor. This surface consists of 10200−5000 solid atoms. The entire surface is modeled in the $x-z$ plane, and the lengths in the x-direction, L_x and z-direction, L_z are both 152.6 Å. All boundaries are set to periodic conditions. We considered three different pillar heights, four different pillar surface fractions, and three different surface energies. The pillars are spaced at regular intervals on the solid surface, and the pillar shape is a regular quadrilateral. W indicates the thickness and width of the pillar in the x-direction and z-direction, as shown in Fig. 1, while H indicates the height.

The thickness of the pillar was increased from 8.48 Å to 21.2 Å, which results in an increase in the pillar surface from 11.1 % to 69.4 %, as shown in Fig. 2. The pillar height was

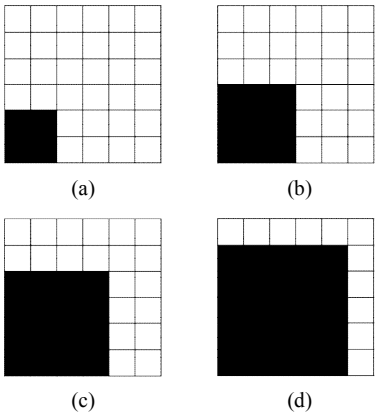

Fig. 2. Schematic view (top view) of variable unit pillar structure and each structure's pillar surface fractions: (a) 11.1 %; (b) 25 %; (c) 44.4 %; (d) 69.4 %.

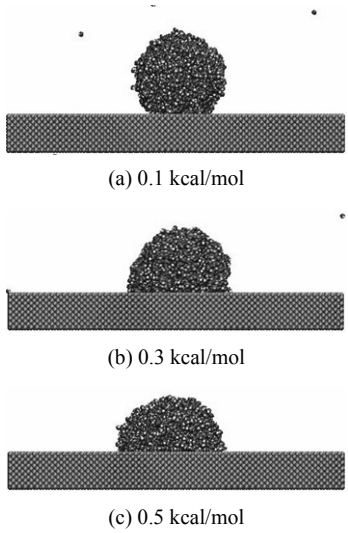

Fig. 3. Snapshots of water droplets on the smooth surface for three different surface energy: (a) γ_s = 4.85 mN/m (ε_S = 0.1 kcal/mol); (b) γ_s = 23.41 mN/m (ε_S = 0.3 kcal/mol); (c) γ_s = 51.78 mN/m (ε_S = 0.5 kcal/mol).

also varied (H = 4.24 Å, 8.48 Å, 12.72 Å). Three different surface energies were controlled by changing the characteristic energy (ε_S = 0.1, 0.3, 0.5 kcal/mol).

To simulate a water droplet on the solid surface, water molecules were initially positioned in a 50 Å × 50 Å × 50 Å cube shape. During the simulation, the water droplet falls toward the solid surface with the nano-structured pillars, and the simulations were run until equilibrium. A time step of 2 fs was used in the 15 ns simulations. After the calculation, the water molecule data were recorded every 2 ps during the last 1 ns and used for post-processing.

The water droplet forms a contact angle on the surface, and it is used to indicate the wetting characteristics [22, 25]. It is measured by considering the density field of the droplet, which is expressed using a density value distribution of 0 to 1. The contact angle is measured at the water droplet's edge where the density had a value of 0.5. In order to ensure accuracy and reliability of the contact angle, it was measured on four sides. There is little difference in the value of the contact angles in the x-direction and z-direction, so the θ_{x-y} and θ_{y-z} contact angles are considered.

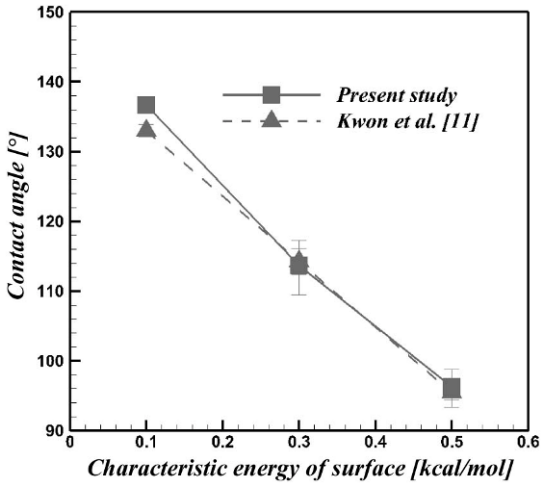

Fig. 4. The validation result of the contact angle as the characteristic energy of surface.

3. Results

At first, the water droplets on smooth surfaces were considered to find the surface energy of each surface with different characteristic energies from 0.1 to 0.5 kcal/mol. Figs. 3(a)-(c) show water droplets on the smooth surfaces. In these cases, the contact angles of the water droplets were 136.68°, 113.66° and 96.29°, respectively. With these contact angles, the surface energies can be calculated using Eq. (5). Therefore the cases with the characteristic energy are rewritten with surface energies of 4.85, 23.41 and 51.78 mN/m.

In order to validate this study, the results were compared with previous numerical results due to the lack of experimental data at this scale. Kwon et al. [26] studied the behavior of water droplets under similar conditions. The number of water molecules was also about 4000 in the previous paper. The smooth surface had a FCC structure and its characteristic energy was from 0.1 kcal/mol to 0.5 kcal/mol. Fig. 4 compares the characteristic energy and contact angle values the previous study and the current study. The figure shows the results were nearly the same so the results of this study are reasonable.

3.1 Surface energy of 4.85 mN/m

Fig. 5 shows images of the $x-y$ view and the $y-z$ view of the water droplet on the pillar surface at the surface energy of 4.85 mN/m (the characteristic energy of 0.1 kcal/mol). The pillars are square with the x and z widths the same ($W_x = W_z$). As the thickness of the pillar increases from 8.48 Å to 21.2 Å, the pillar surface fraction increases from 11.1 % to 69.4 %. Figs. 5(a)-(d) show the shape of the

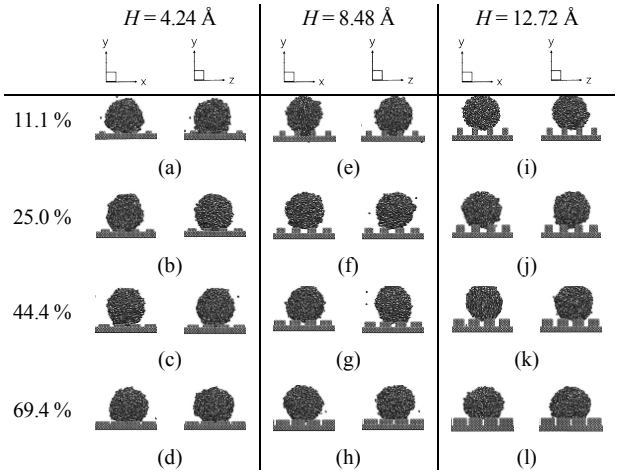

Fig. 5. Snapshots of water droplets on the pillar surface in the $x-y$ view and $y-z$ view with four different pillar surface fraction 11.1 %, 25.0 %, 44.4 %, 69.4 %, and three different pillar height 4.24 Å, 8.48 Å, 12.72 Å when the surface energy is 4.85 mN/m.

water droplet with a low pillar height of H = 4.24 Å and four different pillar surface fractions of 11.1 %, 25 %, 44.4 % and 69.4 %. In these cases, the surfaces are hydrophobic, forming Wenzel state droplets. The water molecules permeate into two gaps between pillars in the $y-z$ view with the pillar surface fraction of 11.1 % and into one and a half gaps in the $x-y$ view with the pillar surface fraction of 25 %. However, at larger pillar surface fractions, water molecules cannot permeate into more than one gap. In other words, the larger the area ratio of the pillar, the less the water molecules permeate between the pillar structures.

Figs. 5(e)-(h) show the water droplet shapes for a pillar height of H = 8.48 Å and the four different pillar surface fractions. In these cases, the surfaces are very hydrophobic, so there is no permeation of water molecules into the gaps except at 11.1 % pillar surface fraction. The water molecules fill one gap in the $x-y$ view and one gap in the $y-z$ view. Figs. 5(i)-(l) show the water droplet shapes for a pillar height H = 12.72 Å. There is little conformational change of the water droplet on the higher pillars since it is in the Cassie-Baxter state. The result is attributed to the stronger attractions between the water molecules than that between the water droplet and the surface base. As a result, the water droplet cannot permeate into the gaps and coheres in a spherical shape on top of the pillars, especially at the 11.1 % and 25 % pillar surface fractions.

Fig. 6 and Table 1 show the contact angles for the pillar surface fractions and pillar heights with a 4.85 mN/m surface energy. The x-axis represents the pillar surface fraction, and the y-axis represents the contact angle of the water droplet. The smooth surface without pillars in Fig. 3(a) is indicated by a pillar surface fraction of 100 % in Fig. 6. The contact angle in this case is 136.7°. The low surface energy of 4.85 mN/m has less attraction on the water droplet, so the contact angle is high.

Table 1. Contact angles for different pillar surface when the surface energy is 4.85 mN/m and the pillar height is 4.24 Å, 8.48 Å, 12.72 Å.

Contact angles (°) : Surface energy 4.85 mN/m						
Pillar surface fractions (%)		11.1	25	44.4	69.4	100
Pillar height (Å)	4.24	134.05	136.01	138.53	136.74	136.68
	8.48	135.68	142.28	139.32	137.37	136.68
	12.72	142.72	142.64	140.04	136.40	136.68

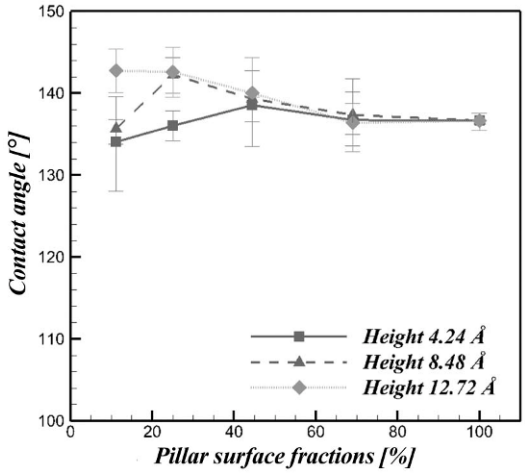

Fig. 6. Contact angles for different pillar surface fractions: x-axis show the variable pillar surface fraction from 11.1 % to 100 % and y-axis shows each case's contact angle when the surface energy is 4.85 mN/m and the pillar height is 4.24 Å, 8.48 Å, 12.72 Å.

At a 4.24 Å pillar height, as the pillar surface fraction increases from 11.1 % to 100 %, the contact angle for each case increases slightly from 134.05° to 138.53° at a pillar surface fraction of 44.4 %, and then it decreases to 136.68°. All of these are Wenzel state cases, it can be seen that the more gaps the droplet fills, the smaller the contact angle is. The peak contact angle is at a pillar surface fraction of 44.4 % where the droplet fills only one gap in the $x-y$ and $y-z$ views. Because of small gaps in high surface fraction, water molecules cannot permeate so most of the water molecules are on top of the structure.

The H = 8.48 Å pillar height cases have a similar trend. As the pillar surface fraction increases from 11.1 % to 100 %, the contact angle first increases and then decreases. For these cases, the peak occurs just after making a transition in state from Wenzel to Cassie-Baxter, which occurs at the pillar surface fraction of 25 %.

The cases with a H = 12.72 Å pillar height are different from those at H = 4.24 Å and H = 8.48 Å. The contact angle is the highest at the pillar surface fraction of 11.1 %, and the contact angle decreases as the pillar surface fraction increases. All of these cases are in the Cassie-Baxter state and the pillars are tall, so the attraction of the base surface has no effect on the water molecules. However, as the pillar surface fraction increases, the gaps between the pillars decrease and

Table 2. Contact angles for different pillar surface when the surface energy is 23.41 mN/m and the pillar height is 4.24 Å, 8.48 Å, 12.72 Å.

Contact angles (°) : Surface energy 23.41 mN/m						
Pillar surface fractions (%)		11.1	25	**44.4**	**69.4**	**100**
Pillar height (Å)	**4.24**	115.81	118.25	119.88	121.54	113.66
	8.48	115.75	124.29	131.19	122.83	113.66
	12.72	125.74	131.11	132.13	121.19	113.66

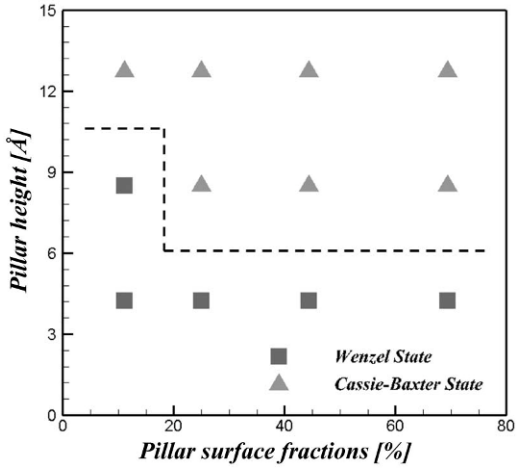

Fig. 7. The map of wetting characteristics when the surface energy is 4.85 mN/m and the pillar height is 4.24 Å, 8.48 Å, 12.72 Å.

the surface appears more and more like a flat surface. This causes the contact angle to decrease.

Fig. 7 shows a map of the wetting characteristics for the surface energy of 4.85 mN/m. There are more cases of the Cassie-Baxter state than the Wenzel state. Many cases in Wenzel state occur at the low pillar height. Low pillars cannot prevent the attraction of the plate. However, high pillars play a role as resistance to water permeation resulting in water droplets being in the Cassie-Baxter state in those cases.

3.2 Surface energy of 23.41 mN/m

The $x-y$ and $y-z$ views of the water droplet are seen in Fig. 8 for the surface energy of 23.41 mN/m (the characteristic energy of 0.3 kcal/mol). Figs. 8(a)-(d) show the shape of the water droplet at H = 4.24 Å and the four different pillar surface fractions. All cases show the permeation of water into two or more gaps in the $x-y$ view and $y-z$ view. Figs. 8(a) and (b) show the water molecule permeation into a third gap when the pillar surface fractions are 11.1 % and 25.0 %.

Figs. 8(e)-(h) show the shape of the water droplet at H = 8.48 Å , and Figs. 8(i)-(l) show the shape at H = 12.72 Å. As the pillar surface fraction increases from 11.1 % to 44.4 %, the water permeation between the gaps decreases. At 69.4 % pillar surface fraction, there is hardly any permeation because the distance between the pillars is very small restricting the infiltration, and water droplets adhere to the surface because the

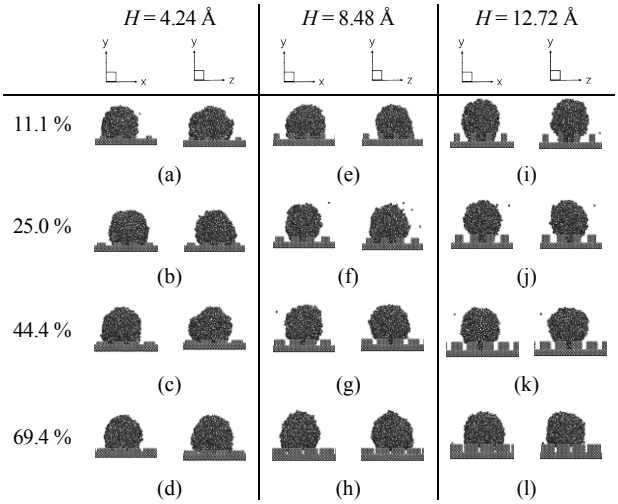

Fig. 8. Snapshots of water droplets on the pillar surface in the $x-y$ view and $y-z$ view with four different pillar surface fraction 11.1 %, 25.0 %, 44.4 %, 69.4 %, and three different pillar height 4.24 Å, 8.48 Å, 12.72 Å when the surface energy is 23.41 mN/m.

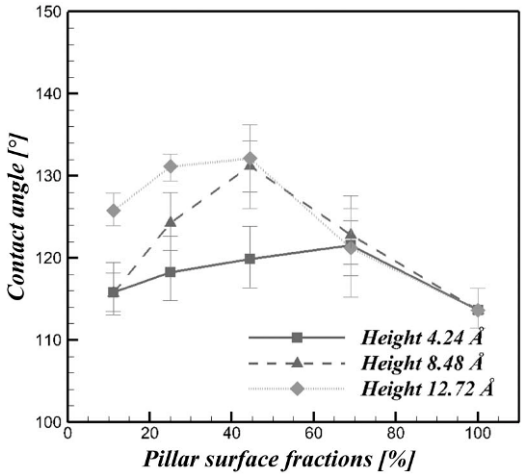

Fig. 9. Contact angles for different pillar surface fractions: x -axis show the variable pillar surface fraction from 11.1 % to 100 % and y -axis shows each case's contact angle when the surface energy is 23.41 mN/m and the pillar height is 4.24 Å, 8.48 Å, 12.72 Å.

surface shape is similar to a smooth surface.

Fig. 9 and Table 2 show the wetting characteristics using the contact angles in Fig. 3(b) and Fig. 8. The variation of the contact angles with the different pillar surface fractions and the pillar heights is seen in Fig. 9 for the surface energy of 23.41 mN/m. The smooth surface without pillars has a pillar surface fraction of 100 % and a contact angle of 113.7°.

The 23.41 mN/m trend is somewhat similar to that of the 4.85 mN/m cases seen in Fig. 6. As the pillar surface fraction increases from 11.1 % to 100 %, the contact angles increase and then decrease. The increase in the pillar surface fraction causes the permeation of the water molecules to decrease, and more of the water droplet sits on the top of the surface. This increases the contact angle. However, with larger pillar surface fractions, the contact angle decreases because the surface

Table 3. Contact angles for different pillar surface when the surface energy is 51.78 mN/m and the pillar height is 4.24 Å, 8.48 Å, 12.72 Å.

Contact angles (°) : Surface energy 51.78 mN/m						
Pillar surface fractions (%)		11.1	25	44.4	69.4	100
Pillar height (Å)	4.24	84.93	90.49	91.99	99.72	96.29
	8.48	75.48	81.12	92.35	94.41	96.29
	12.72	84.14	102.99	103.42	101.49	96.29

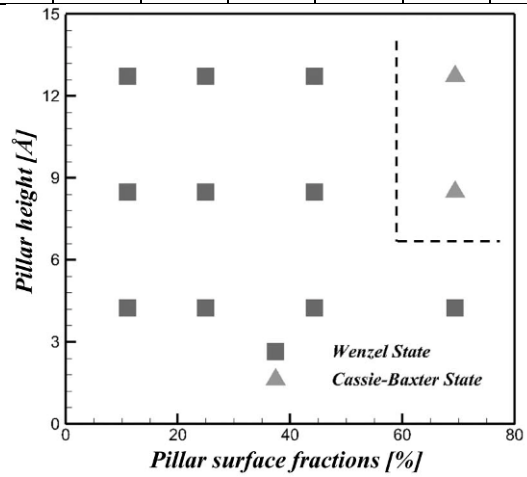

Fig. 10. The map of wetting characteristics when the surface energy is 23.41 mN/m and the pillar height is 4.24 Å, 8.48 Å, 12.72 Å.

shape becomes more like a smooth surface. This effect is much stronger than the one that increases the contact angle due to the narrowing gaps preventing water molecules from permeating between the pillars. As a result, the attraction between the water droplet and the surface is greater than that between the water molecules, and the contact angle becomes smaller at larger pillar surface fractions.

Fig. 10 shows a map of the wetting characteristics for the surface energy of 23.41 mN/m. In this condition, almost all cases were in the Wenzel state. There are only two cases in the Cassie-Baxter state. Because of the increased surface energy, the attraction between the water molecules and the pillars increases so that pillars cannot act as resistance to water permeation. As a result, the effect of pillars on the state of the water droplet decreases as the surface energy of the solid surface increases.

3.3 Surface energy of 51.78 mN/m

The $x-y$ view and the $y-z$ view of the water droplet can be seen in Fig. 11 for the surface energy of 51.78 mN/m (the characteristic energy of 0.5 kcal/mol). Figs. 11(a)-(h) show the water droplet shape for the different cases at H = 4.24 Å and H = 8.48 Å. Overall, there is permeation into the gaps of the pillars in all cases in the $x-y$ view and $y-z$ view. Figs. 11(i)-(l) show the shape for at H = 12.72 Å. In these cases, there is a different tendency with different permeation from the cases at H = 4.24 Å and 8.48 Å. Two to three gaps are filled, and the taller pillars prevent the water molecules from running over into three gaps.

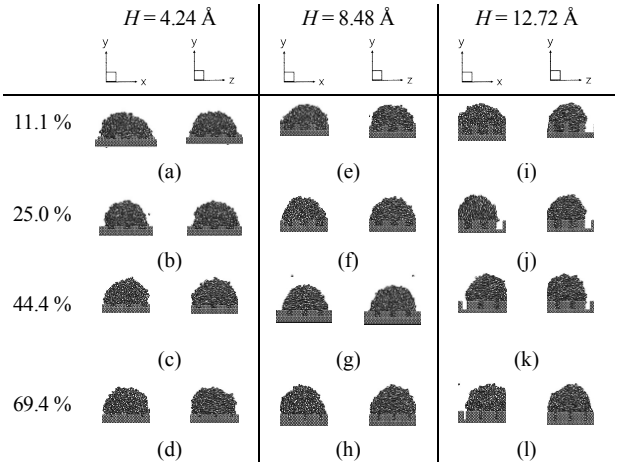

Fig. 11. Snapshots of water droplets on the pillar surface in the $x-y$ view and $y-z$ view with four different pillar surface fraction 11.1 %, 25.0 %, 44.4 %, 69.4 %, and three different pillar height 4.24 Å, 8.48 Å, 12.72 Å when the surface energy is 51.78 mN/m.

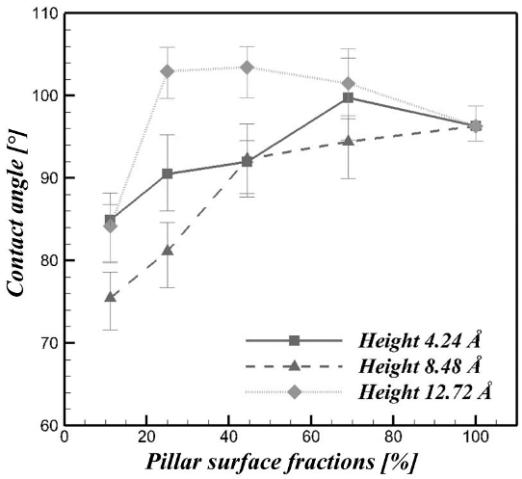

Fig. 12. Contact angles for different pillar surface fractions: x-axis show the variable pillar surface fraction from 11.1 % to 100 % and y-axis shows each case's contact angle when the surface energy is 51.78 mN/m and the pillar height is 4.24 Å, 8.48 Å, 12.72 Å.

Fig. 12 and Table 3 show the wetting characteristics using the contact angles in Figs. 3(c) and 11. The variation of the contact angles at a surface energy of 51.78 mN/m is seen in Fig. 12. The smooth surface without pillars, the pillar surface fraction of 100 %, has a contact angle of 96.3°. Generally, there are small contact angles that result from the high attrac tion at this surface energy.

For each pillar height, the lowest contact angle occurs at the smallest pillar surface fraction. The reason is that with a larger surface energy and small pillar surface fraction, a large share of the droplet sinks into gaps of the pillars, which decreases the contact angle and making the surface more hydrophilic. Except at the 8.48 Å pillar height, as the pillar surface fraction

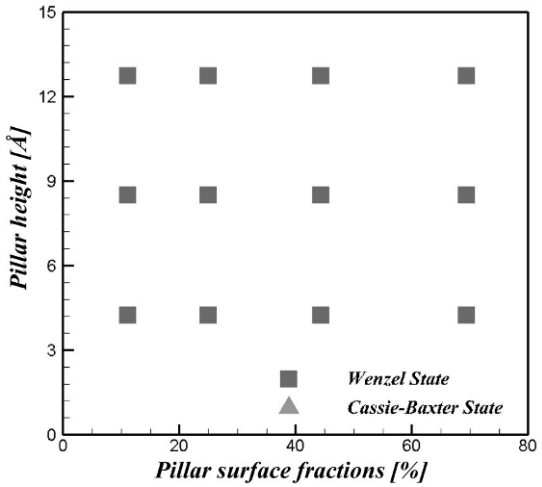

Fig. 13. The map of wetting characteristics when the surface energy is mN/m and the pillar height is 4.24 Å, 8.48 Å, 12.72 Å.

increases, the contact angle increases and then decreases. At H = 8.48 Å, as the gaps decrease, fewer water molecules permeate the gaps, and the contact angle increases. At H = 4.24 Å, the contact angles are larger than at H = 8.48 Å. The reason is that the added mass of the high surface energy pillars attract more water to the surface, and the gaps at H = 8.48 Å are deeper than those at H = 4.24 Å, so more water is pulled into the gaps. This reduces the contact angle if the same number of gaps are filled. However, with H = 12.72 Å pillars, even though the gaps are even deeper, the droplet does not fill three gaps in both the $x-y$ and $y-z$ views in any cases. The smaller number of gaps filled produces a higher contact angle. Furthermore, the peak contact angles occur at the pillar surface fractions of 25 % and 44.4 %, where the water droplet fills only two gaps in both the $x-y$ and $y-z$ views.

Fig. 13 shows the map of wetting characteristics at this surface energy. All of the cases are in the Wenzel state. Due to the large surface energy, the pillars also attract the water molecules so that the water molecules can permeate the gaps easier than those of the other cases.

4. Conclusions

The wetting characteristics of various pillar surfaces were evaluated using molecular dynamics simulation. Regular quadrilateral pillars with different pillar surface fractions, surface energies, and pillar heights were considered to compare the wetting characteristics of various pillar surfaces.

For the surface energy of 4.85 mN/m with pillar heights of 4.24 Å and 8.48 Å, the contact angle of water droplet slightly increases and has the largest value at the pillar surface fraction of 25 % or 44.4 %. The contact angle decreases as the pillar surface fraction increases. However, the case for the pillar height of H = 12.72 Å shows a different trend. In this case, the contact angle gradually decreases as the pillar surface fraction increases.

At the surface energy of 23.41 mN/m, the results show the similar trend comparing with those at the surface energy of 4.85 mN/m and low pillar height. The contact angle increases and then decreases as the pillar surface fraction increases. However, in these cases, the peak contact angles are seen at the pillar surface fraction of 44.4 % or 69.4 % which are larger than those in the case with the surface energy 4.85 mN/m.

At the largest surface energy, 51.78 mN/m, with the pillar heights of H = 4.24 Å and 8.48 Å, the contact angles become larger as the pillar surface fraction increases. However, at H = 12.72 Å, the peak contact angles occur at pillar surface fractions of 25 % and 44.4 %.

The contact angles and wetting characteristics of the water droplets on the surface are dependent on the surface energy as well as the pillar characteristics such as pillar the surface fraction and pillar height. This study may give some guidelines to control the wetting characteristics of surfaces according to the pillar characteristics.

Acknowledgment

This research was supported by Basic Science Research Program through the National Research Foundation of Korea (NRF) funded by the Ministry of Education, Science and Technology (NRF-2017R1A2B3004883). This subject is supported by Korea Ministry of Environment (MOE) as "the Chemical Accident Prevention Technology Development Project".

Nomenclature

W_x	: x-direction pillar edge
W_z	: z-direction pillar edge
H	: Pillar height
r_{ij}	: Distance between atom i and atom j
ε_S	: Lennard-Jones characteristic energy of the surface
ε_{ij}	: Lennard-Jones characteristic energy between atom i and atom j
σ_{ij}	: Lennard-Jones characteristic length between atoms i and j
γ	: Surface energy of the surface
θ	: Contact angle of the droplet

References

[1] Y. C. Jung and B. Bhushan, Biomimetic structures for fluid drag reduction in laminar and turbulent flows, *Journal of Physics : Condensed Matter*, 22 (3) (2009) 035104.

[2] Y. Su, B. Ji, Y. Huang and K. Hwang, Nature's design of hierarchical superhydrophobic surfaces of a water strider for low adhesion and low-energy dissipation, *Langmuir*, 26 (2010) 18926-18937.

[3] X. Q. Bai, G. T. Xie, H. Fan, Z. X. Peng, C. Q. Yuan and X. P. Yan, Study on biomimetic preparation of shell surface microstructure for ship antifouling, *Wear*, 306 (2013) 285-

295.
[4] J. Genzer and A. Marmur, Biological and synthetic self-cleaning surfaces, *Mrs Bulletin*, 33 (2008) 742-746.
[5] Y. S. Kong and T. W. Kim, Wettability of biomimetic riblet surface like sharkskin, *Journal of the Korean Society of Tribologists and Lubrication Engineers*, 29 (2013) 304-309.
[6] R. N. Wenzel, Resistance of solid surfaces to wetting by water, *Industrial & Engineering Chemistry*, 28 (1936) 988-994.
[7] A. B. D. Cassie and S. Baxter, Wettability of porous surfaces, *Transactions of the Faraday Society*, 40 (1944) 546-551.
[8] C. Yang, U. Tartaglino and B. N. J. Persson, Influence of surface roughness on superhydrophobicity, *Physical Review Letters*, 97 (2006) 116103.
[9] G. Carbone and L. Mangialardi, Hydrophobic properties of a wavy rough substrate, *The European Physical Journal E*, 16 (1) (2005) 67-76.
[10] L. W. Schwartz and S. Garoff, Contact angle hysteresis on heterogeneous surfaces, *Langmuir*, 1 (1985) 219-230.
[11] D. M. Spori, T. Drobek, S. Zürcher, M. Ochsner, C. Sprecher, A. Mühlebach and N. D. Spencer, Beyond the lotus effect: Roughness influences on wetting over a wide surface-energy range, *Langmuir*, 24 (2008) 5411-5417.
[12] S. H. Yang, M. Nasonovsky, H. Zhang and K. Chung, Nanoscale water capillary bridges under deeply negative pressure, *Chemical Physics Letters*, 451 (2008) 88-92.
[13] R. Kannan and D. Sivakumar, Drop impact process on a hydrophobic grooved surface, *Colloids and Surfaces*, 317 (2008) 694-704.
[14] T. J. Hirvi and T. A. Pakkanen, Molecular dynamics simulations of water droplets on polymer surfaces, *The Journal of Chemical Physics*, 125 (2006) 144712.
[15] M. Lundgren, N. L. Allan and T. Cosgrove, Molecular dynamics study of wetting of a pillar surface, *Langmuir*, 19 (2003) 7127-7129.
[16] Z. Guo, F. Zhou, J. Hao and W. Liu, Stable biomimetic super-hyprophobic engineering materials, *Journal of American Chemical Society*, 127 (2005) 15670-15671.
[17] X. Gao and L. Jiang, Water-repellent legs of water striders, *Nature*, 32 (2004) 36.
[18] F. Bai, J. Wu, G. Gong and L. Guo, Biomimetic "water strider leg" with highly refined nanogroove structure and remarkable water-repellent performance, *ACS Applied Materials & Interfaces*, 6 (18) (2014) 16237-16242.
[19] T. Koishi, K. Yasuoka, S. Fujikawa, T. Ebisuzaki and X. C. Zeng, Coexistence and transition between Cassie and Wenzel state on pillared hydrophobic surface, *Proceedings of the National Academy of Sciences of the United States of America*, 106 (21) (2009) 8435-8440.
[20] D. Murakami, H. Jinnai and A. Takahara, Wetting transition from the Cassie-Baxter state to the Wenzel state on textured polymer surfaces, *Langmuir*, 30 (2014) 2061-2067.
[21] M. S. Ambrosia, M. Y. Ha and S. Balachandar, The effect of pillar surface fraction and pillar height on contact angles using molecular dynamics, *Applied Surface Science*, 282 (2013) 211-216.
[22] W. J. Jeong, M. Y. Ha, H. S. Yoon and M. Ambrosia, Dynamic behavior of water droplets on solid surfaces with pillar-type nanostructures, *Langmuir*, 28 (2012) 5360-5371.
[23] C. Phillips, R. Braun, W. Wang, J. Gumbart, E. Tajkhorshid, E. Villa, C. Chipot, R. D. Skeel, L. Kale and K. Schulten, Scalable molecular dynamics with NAMD, *Journal of Computational Chemistry*, 26 (16) (2005) 1781-1802.
[24] D. K. Owens, Estimation of the surface free energy of polymers, *Journal of Applied Polymer Science*, 13 (1969) 1741-1747.
[25] C. W. Extrand, Model for contact angles and hysteresis on rough and ultraphobic surfaces, *Langmuir*, 18 (2002) 7991-7999.
[26] T. W. Kwon, M. S. Ambrosia, J. Jang and M. Y. Ha, Dynamic hydrophobicity of heterogeneous pillared surfaces, *Journal of Mechanical Science and Technology*, 29 (4) (2015) 1663-1671.

Man-Yeong Ha received his B.S. degree from Pusan National University, Korea, in 1981, M.S. degree, in 1983, from Korea Advanced Institute of Science and Technology, Korea, and Ph.D. degree from Pennsylvania State University, USA in 1990. Dr. Ha is currently a Professor at the School of Mechanical Engineering at Pusan National University in Busan, Korea. He serves as an Editor of the Journal of Mechanical Science and Technology. His research interests are focused on thermal management, computational fluid dynamics, and micro/nano fluidics.

Min Jung Yoo received her B.S. degree from Dongduk Women's University, Korea, in 2015. She received her master degree under the supervision of Prof. Man-Yeong Ha. Her research interests are focused on micro/nano fluidics and surface control using molecular dynamics.